Surface evolution of salt-encrusted playas under extreme and continued dryness

Journal:	*Earth Surface Processes and Landforms*
Manuscript ID:	Draft
Wiley - Manuscript type:	Paper
Date Submitted by the Author:	n/a
Complete List of Authors:	Artieda, Octavio; Universidad de Extremadura, Department of Vegetal Biology, Ecology and Earth Science Dávila, Alfonso; NASA, Ames Research Center Wierzchos, Jacek; Museo Nacional de Ciencias Naturales-CSIC, Biogeochemistry and Microbial Ecology Buhler, Peter; California Institute of Technology, Division of Geological and Planetary Sciences Rodríguez-Ochoa, Rafael; Universitat de Lleida, Dept. Medi Ambient i Ciències del Sòl Pueyo, Juan; University of Barcelona, Faculty of Geology Ascaso, Carmen; Museo Nacional de Ciencias Naturales-CSIC, Biogeochemistry and Microbial Ecology
Keywords:	Atacama Desert, Halite, Aridity, Salar evolution, Salt Polygons

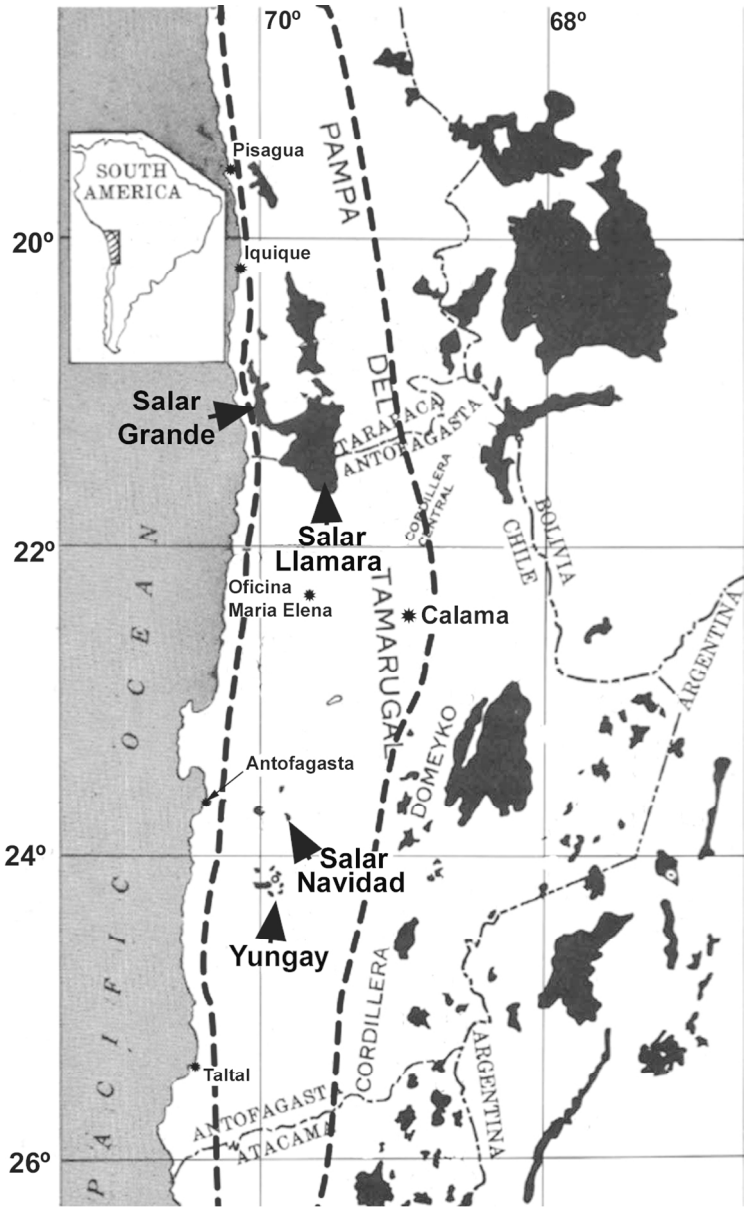

Figure 1. Map of northern Chile showing the distribution of salars (black areas), according to Stoertz and Ericksen (1974). The dashed lines delimit the hyperarid Central Valley, which contains fossil salars. The study sites in the Central Valleys are marked with arrowheads.
98x158mm (300 x 300 DPI)

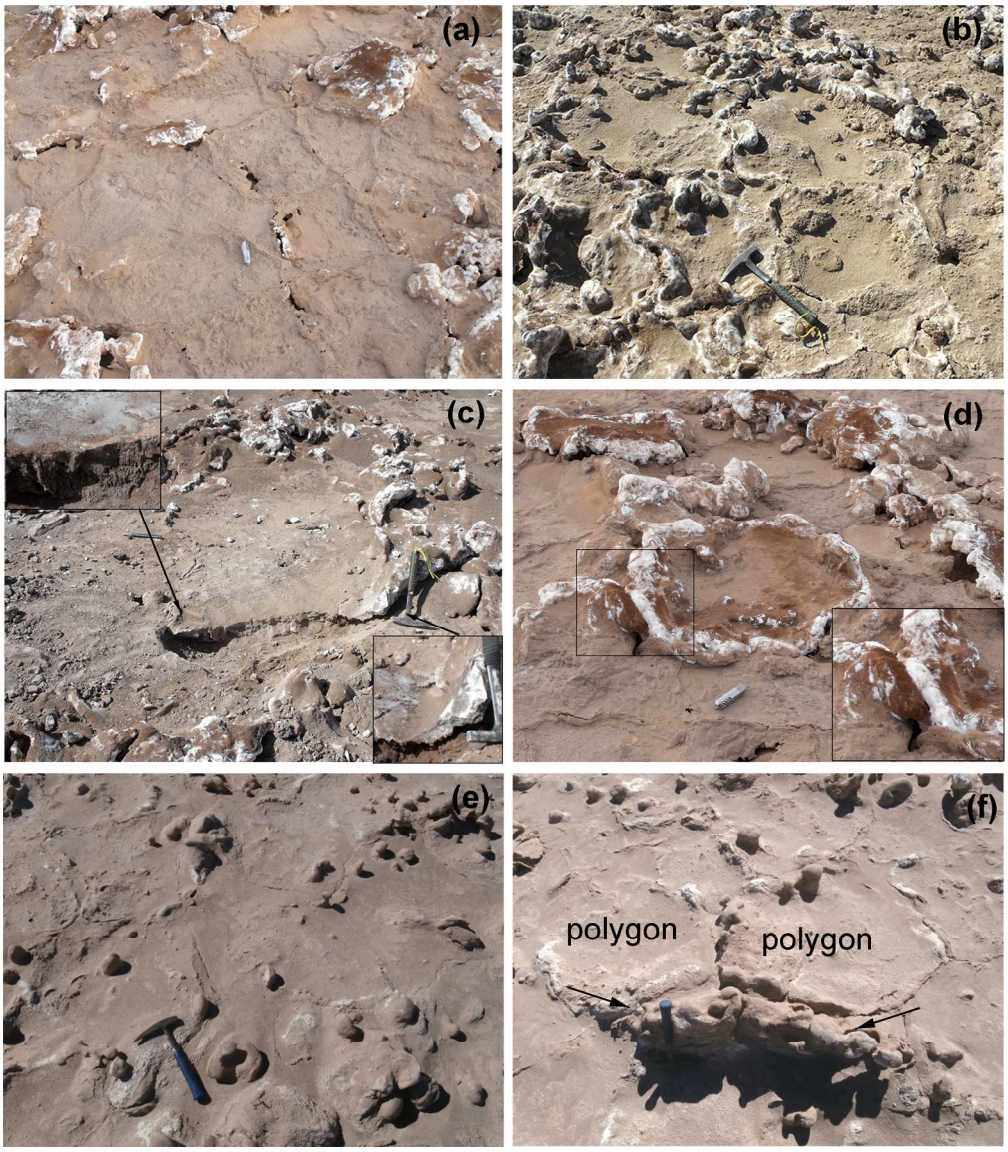

Figure 2. Morphology of salt polygons. (a): Type I polygons represent an initial stage of dry salt encrusted playa which likely become a remnant feature due to salt starvation. These polygons are flat and well defined with slightly elevated rims that are sealed together with the rims of adjacent polygons (pocket knife for scale); (b-d) Type II polygons represent intermediate stages of polygon evolution under extreme and prolonged dryness. Type II polygons are characterized by a regular, concave shape, uplifted rims, and salt enrichments along polygon borders. Depending on the degree of evolution of salt nodules along the polygon borders we distinguish early stage Type II polygons (poorly developed nodules) and late stage Type II polygons (well developed nodules); (e) and (f): Type III polygons represent a final stage of polygon evolution under extreme and prolonged dryness, with poorly defined borders, which are occasionally rounded or irregular, and well-developed nodules along the polygon sides. Occasionally the polygons are almost vertically oriented, forming uplifted fin-like structures (arrows).
219x250mm (300 x 300 DPI)

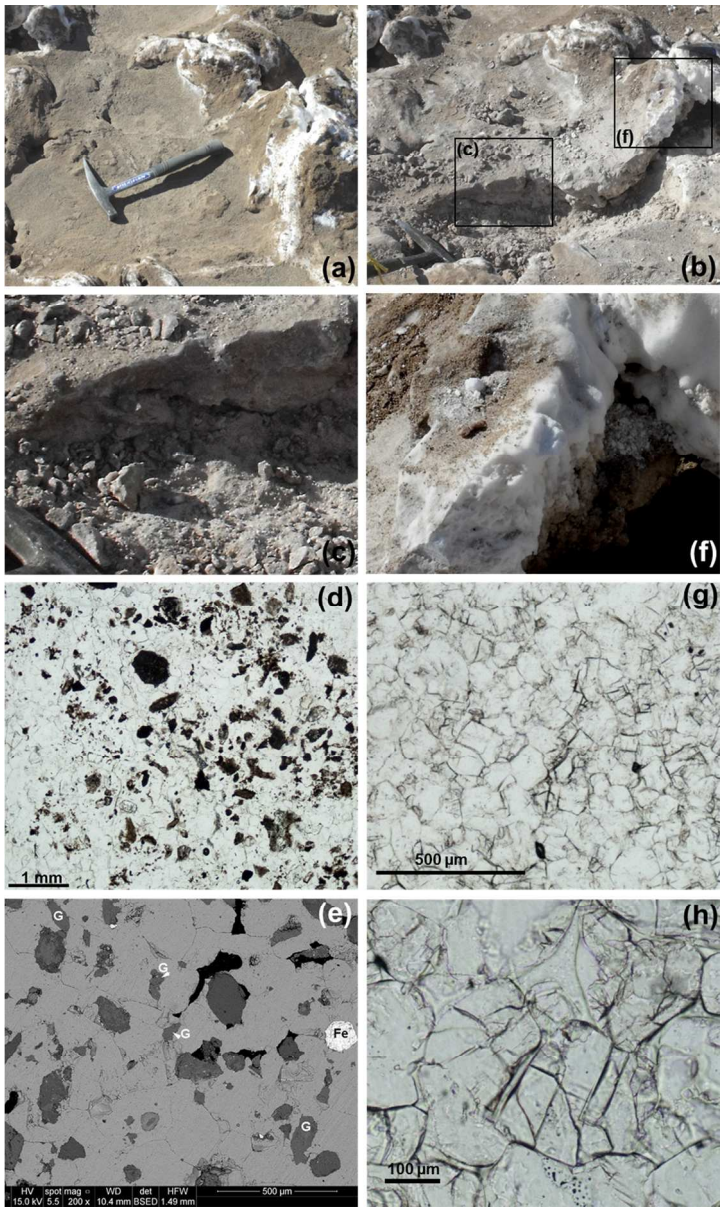

Figure 3. Differences in structure and mineralogy between polygon centers and borders. (a): Type III polygon viewed in the field (Salar Grande). (b) Cross-sectional view of polygon in (a). (c): Detail of the central region of the polygon in (b). (d): Photomicrograph under plane-polarized light of sample ATAC-33 (Salar Grande), corresponding to the center of the polygon. Note the halite mass containing detrital grains of different composition (feldspars, iron oxides). (e): SEM-BSE image of sample ATAC-33. Note the gypsum crystals with irregular morphology and iron oxides {Fe}. (f): Field photo of the border material from the polygon in (b). Note the mineral purity of the halite (free from detrital material). (g): Photomicrograph under plane-polarized light of sample ATAC-32 (Salar Grande), corresponding to the border of the polygon in (f). The sample is composed almost entirely of halite and gypsum. The halite crystals form a mosaic with both straight and rounded borders, as can be seen in detail (h).
150x251mm (300 x 300 DPI)

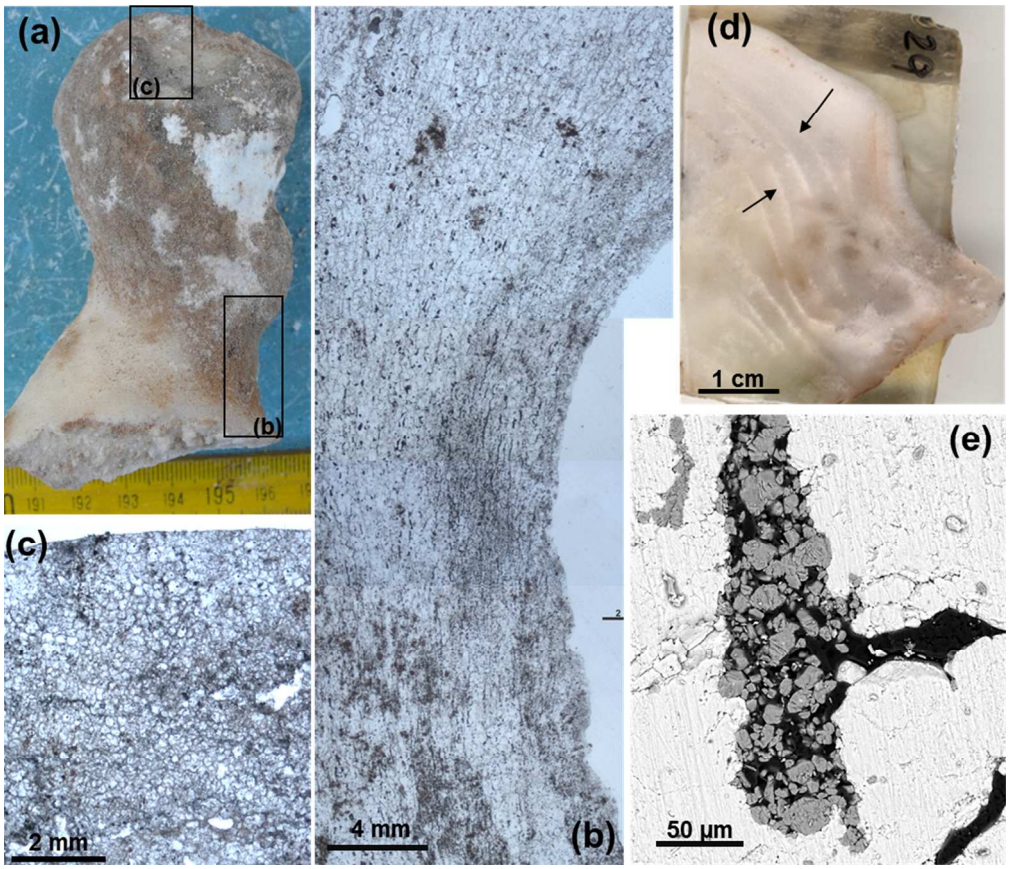

Figure 4. (a) Field photo of a halite nodule (Salar Llamara, Sample ATAC-21). (b) Lines of elongated voids parallel to the boundary of the nodule in thin section of sample ATAC-21. Note the contrast between the voids and the crystallographic and pore fabric composing the bulk of the nodule, as seen in (c). Both (b) and (c) are photomicrographs under plane-polarized light. (d): Polished section of a nodule (sample ATAC-29, Salar Grande). Note the banding subparallel to the surface. (e): The banding in (d) corresponds to elongated pores partially filled in with <20 micrometer subhedral gypsum crystals (SEM-BSE image).
250x214mm (300 x 300 DPI)

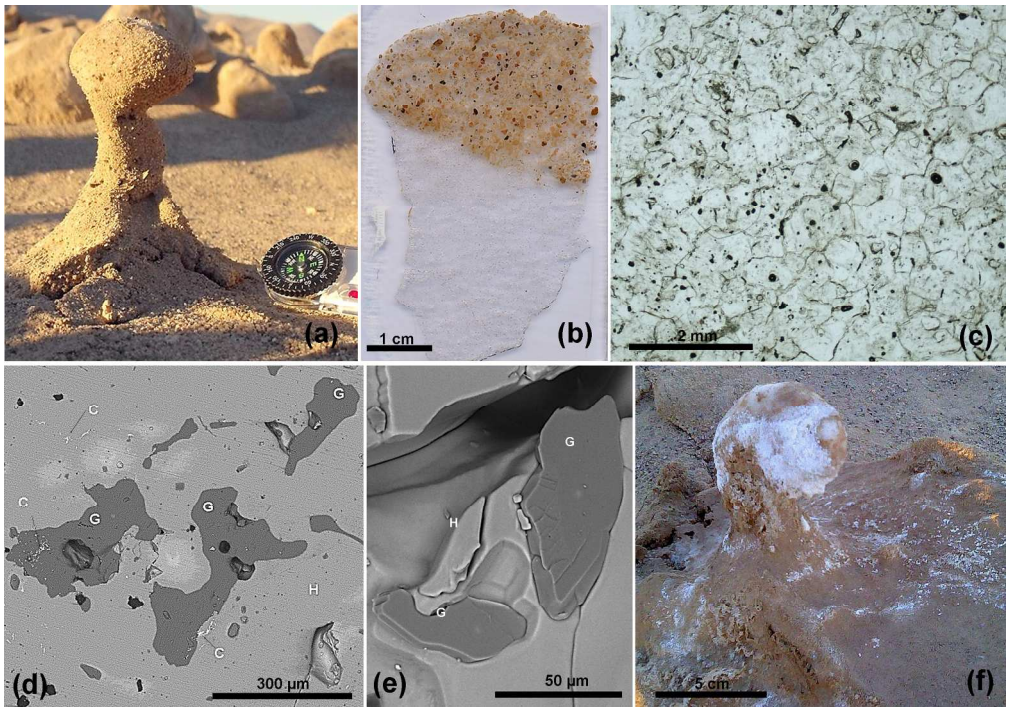

Figure 5. (a) Halite nodule covered with abundant detrital grains. (b): Polished section of the nodule in (a). Note the color contrast marking the contact between the upper zone, composed of detrital grains, and the lower zone, composed exclusively of halite. (c): Photomicrograph of the lower zone of the nodule under plane-polarized light. (d) and (e): SEM-BSE images of amoeboid inclusions of gypsum in halite (G: gypsum, H: halite, C: celestite). (f): Halite nodule with surface efflorescence.
250x174mm (300 x 300 DPI)

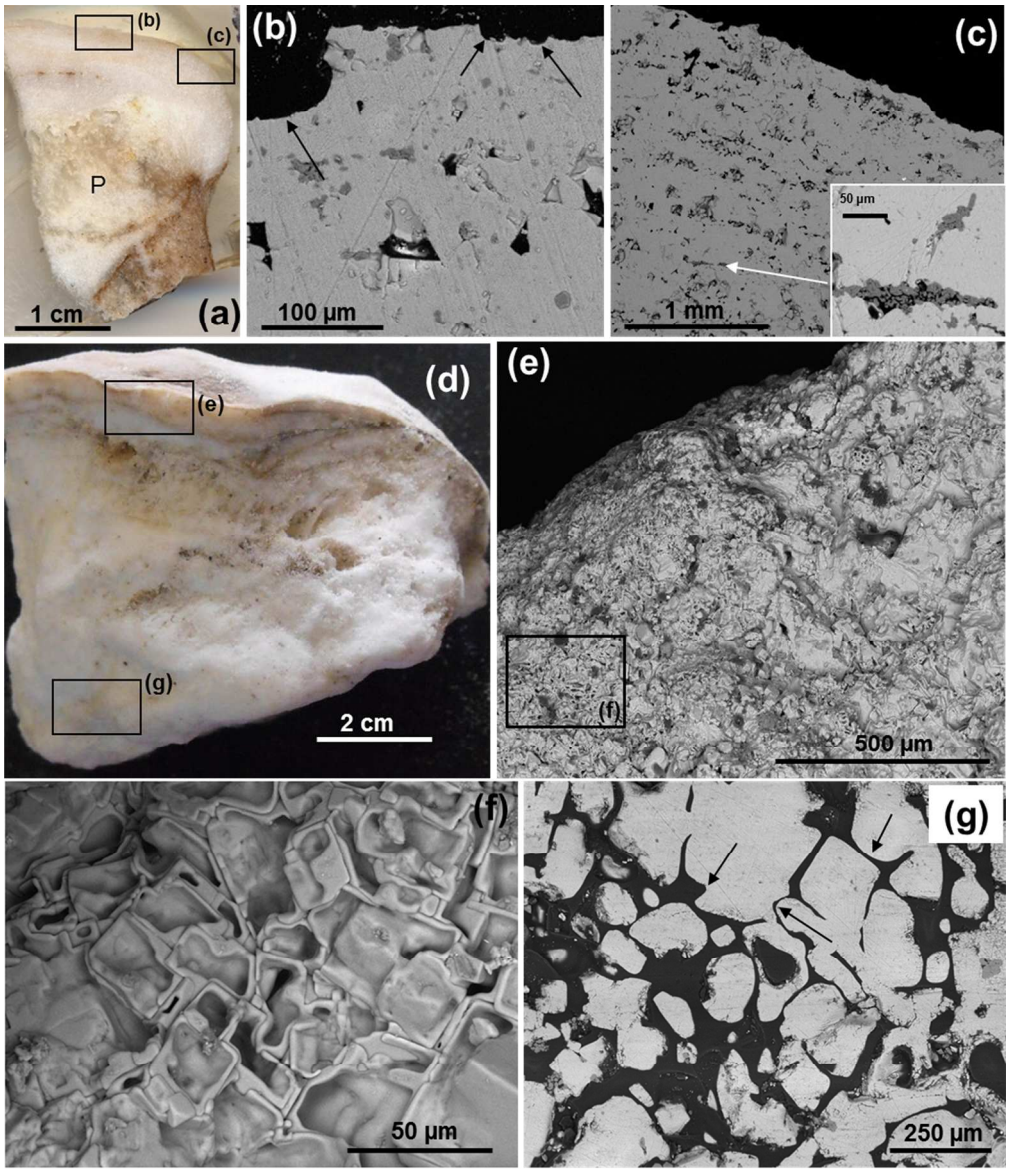

Figure 6. (a) Polished section of halite nodule (ATAC-5). Note the porous zone (P) that is characteristic of the nodule cores, the lineation subparallel to the external surface of the nodule, and that the surface is encrusted with a millimeter-scale layer composed almost exclusively of halite. (b): SEM-BSE image of sample surface shown in (a); note the dissolution features on the surface (arrows). (c): SEM-BSE image of pore clusters arranged along lines parallel to the surface are present in the outer zone of the nodule shown in (a); some of the pores are partially filled in by gypsum crystals. (d): Another example of a nodule with a laminated, dense outer shell a few millimeters thick (sample ATAC-310b). (e): SEM image of zoomed in view of the crust in (d). This region is dominated by hollow-faced halite crystals, clearly seen in detail in SEM image in fig. (f). (g): SEM-BSE image of halite crystals in the core of the nodule shown in (d), highlighting the presence of rounded crystal boundaries (arrows) and the elevated porosity of this zone.
209x243mm (300 x 300 DPI)

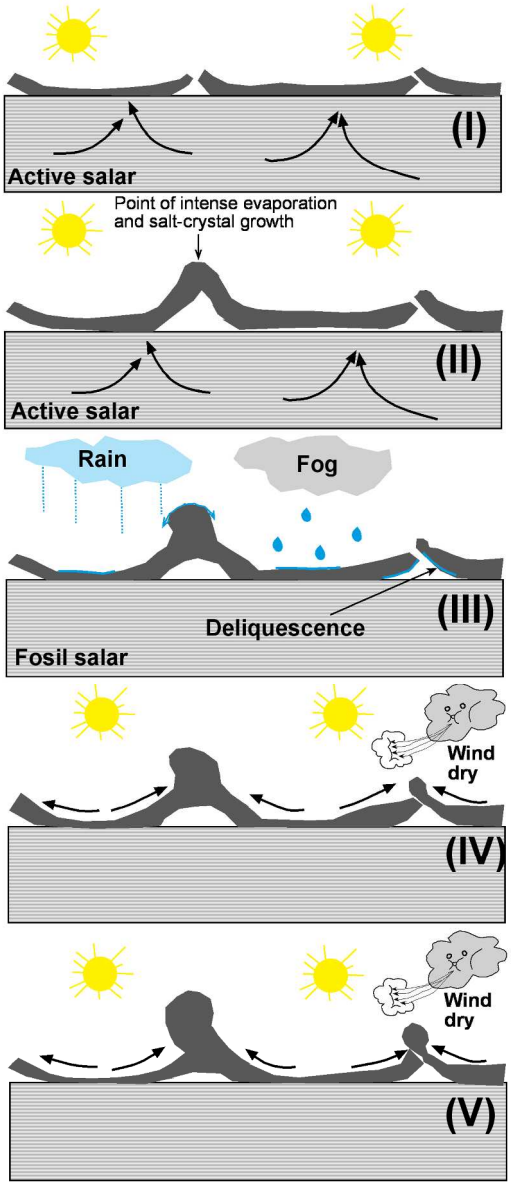

Figure 7. Proposed model to explain the evolution of salt polygons and the genesis of halite nodules in the Atacama Desert: (I) Lateral polygon growth due to subsurface upwelling of halite. (II) Lateral polygon competition and lift-off. Enhanced growth along the edges of the polygons. (III) Water from rain, fog and deliquescence initiates both the dissolution of halite in the center of the polygon and dissolution of the high rims; (IV) and (V) Halite is dissolved by water from rain, fog and deliquescence. The brine then travels along a moisture gradient, which occurs because the uplifted polygon borders experience higher rates of evaporation than the lower, central parts of the polygon, since the uplifted borders are exposed to higher rates of wind desiccation. As the water on the polygon borders evaporates, halite re-precipitates on the highest elevated regions of the rim and eventually grows into nodules.
118x258mm (300 x 300 DPI)

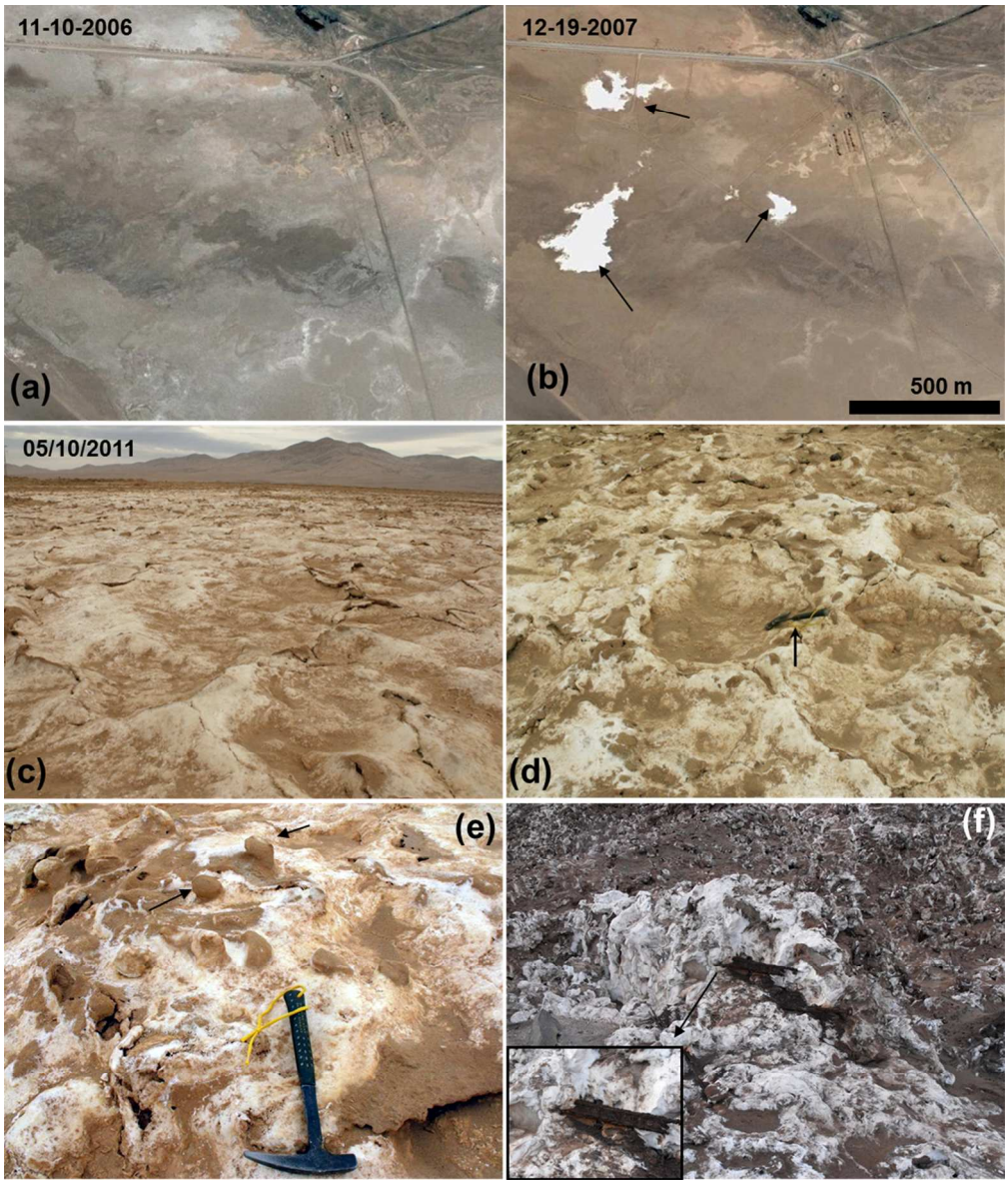

Figure 8. Recent accumulations of halite in Yungay. (a): View in 2006 of the region affected by flooding in 2007, seen in (b). (b): Arrows denote locations (white) affected by flooding from a leaking water pipe in 2007. (c) and (d): Salt accumulation in the white regions marked with arrows in (b). Note the uplifted borders of the salt polygons (the arrow in (b) indicates the hammer) (e) Small nodules that developed on an older generation of polygons (marked with arrows). (f) Halite covering a piece of railroad track to the abandoned Guanillos mine (location: south of Salar Grande).
219x257mm (300 x 300 DPI)

Figure 9. A protrusion on the edge of a polygon in Salar Grande was covered with sterile gauzes in May, 2009 (left panel). The right panel shows the same gauzes, two years later, now covered under the accumulation of halite.
250x92mm (300 x 300 DPI)

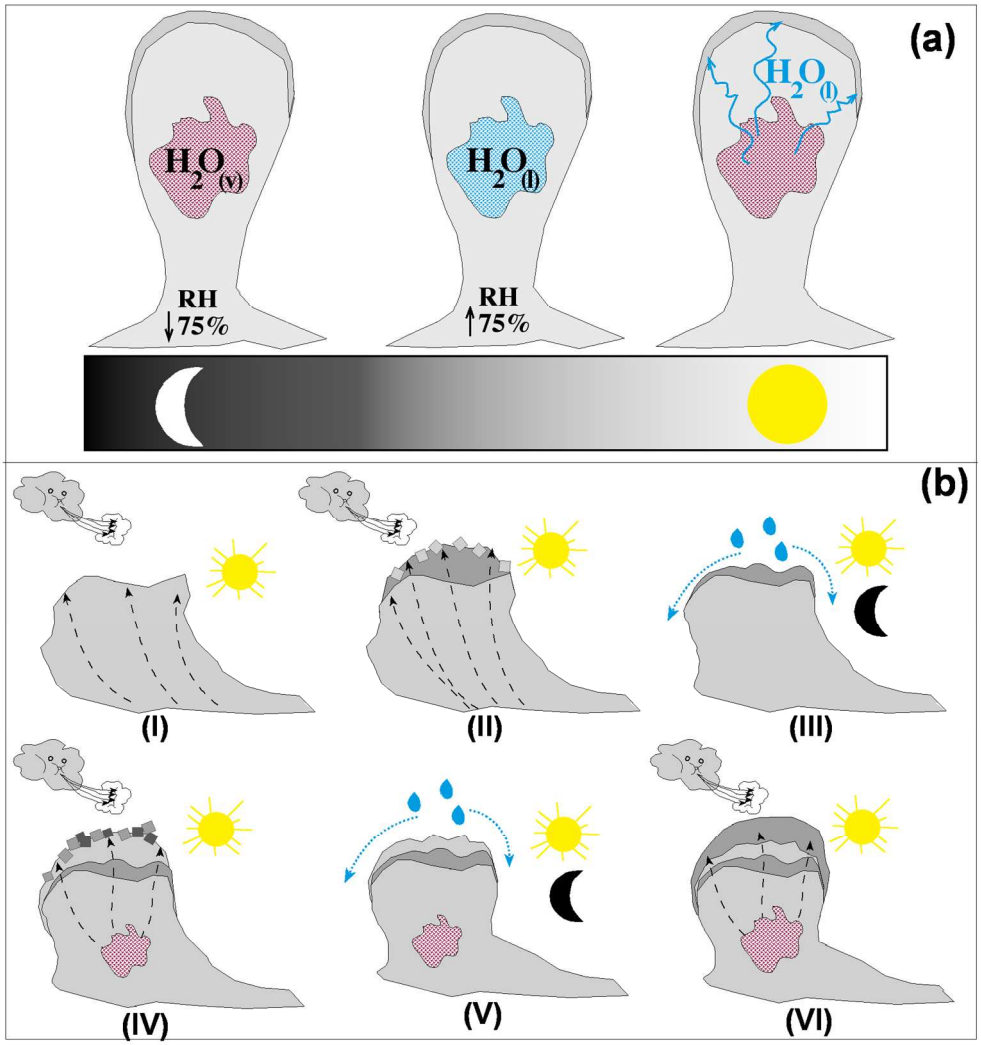

Figure 10. Suggested model to explain the genesis of halite nodules in halite crusts in the Atacama Desert. (a) Water penetrates into the interior of the nodule as a vapor, H2O (v). During the night the temperature drops, raising the relative humidity, which occasionally reaches 75%. At 75% relative humidity deliquescence is initiated, dissolving the halite in the interior of the nodule (capillary condensation might occur at RH < DRH). During the day the ambient temperature rises, initiating evaporation of the water near the surface and driving both capillary migration of briny water and water vapor diffusion from the interior of the nodule to its surface, where the water evaporates and halite precipitates. (b) During the day, wind enhances the evaporation process and contributes to the desiccation of the nodules (I and VI). When briny water reaches the outer layer of the nodule, halite precipitates forming a fresh efflorescence (II and IV). Rapid evaporation by wind action would explain the formation of hollow-faced halite crystals in the outer layers of the salt nodule (II and IV). Sporadic and rare fog or rain events can also reshape the salt nodules (III and V). These processes are cyclical and explain the small porosity of halite nodules surface zone and high porosity within the salt nodule, and their mechanism of formation.
199x211mm (300 x 300 DPI)

Surface evolution of salt-encrusted playas under extreme and continued dryness

Artieda, O[1].; Davila, A[2].F.; Wierzchos, J[3].; Buhler, P.B[4].; Rodríguez-Ochoa, R[5].; Pueyo, J.J[6]. and Ascaso, C[3].

[1]Universidad de Extremadura, 10600 Plasencia, Spain

[2]NASA Ames Research Center, Moffett Field, CA, USA 94035

[3]Museo Nacional de Ciencias Naturales, MNCN-CSIC, 28006 Madrid, Spain

[4]California Institute of Technology, Pasadena, CA, USA 91125

[5]Dept. Medi Ambient i Ciències del Sòl, Universitat de Lleida, 25198 Lleida, Spain

[6]Facultat de Geologia, Universitat de Barcelona, 08071 Barcelona, Spain

Keywords: Salar evolution, Atacama Desert, halite, aridity, salt polygons

Abstract

Miocene continental saltpans are scattered in the Central Valley of the Atacama Desert, one of the driest regions on Earth. These evaporitic deposits are hydrologically inactive, and are detached from groundwater brines or aquifers. The surface of the saltpans, also known as salars, comprises desiccation polygons, often with nodular salt structures along their sides. The morphology and bulk mineralogy of salt polygons differs between and within salars, and the shape and internal structure of salt nodules varies between different polygon types. Based on field observation, and mineralogy and crystallography data, we generated a conceptual model for the genesis and evolution of these surface features, whereby rare rainfall events are responsible for the transformation of desiccation salt polygons and the initial formation of salt nodules along polygon borders. In addition, frequent, but less

intense, deliquescence events further drive the evolution of salt nodules, resulting in a characteristic internal structure that includes laminations, and changes in porosity and crystal morphologies. As a result, and despite the extreme dryness, the surfaces of fossil salars are dynamic on timescales of several years to decades, in response to daily cycles in atmospheric moisture, and also to rare and meager rainfall events. We propose that fossil salars in the Atacama Desert represent an end stage in the evolution of evaporitic deposits under extreme and prolonged dryness.

1. Introduction

The Atacama Desert extends across 1000 km, from 30°S to 20°S, along the Pacific coast of South America (Figure 1). Geological evidence and soil mineralogy suggest that extreme arid conditions have persisted in the southern Atacama for >10–15 million years (Stoertz & Ericksen, 1974; Ericksen 1983; Houston and Hartley, 2003; Dunai et al., 2005; Clarke, 2006). The driest parts of the desert are located between approximately 22°S to 26°S, in the broad valley between the Coastal Range and the Cordillera de Domeyko (Figure 1), also known as the Central Valley, with mean annual precipitation below 1 mm/yr in the driest parts (McKay et al., 2003).

Extreme and continued dryness has resulted in the formation and preservation of large continental salt-encrusted playas, or “salars” (Stoertz & Ericksen, 1974; Chong, 1988; Ericksen & Salas, 1990; Pueyo et al., 2001). Salars are common geomorphological features in the Atacama Desert (s.l.), of which there are approximately 100 reported occurrences clustered in three distinct regions: (1) the Coastal range and Central Valley, between 1000 and 2000 m elevation, (2) the Andean front, between 2000 and 3000 m elevation, and (3) the Andean Altiplano, between 3000 and 5000m elevation. Salt-encrusted playas in the Andean front and the Altiplano are hydrologically active, and host scattered small ponds and lakes that repeatedly cycle through a sequence of stages: from desiccation to flooding to evaporative concentration, following the classic cycle of ephemeral saltpans (Lowenstein and Hardie, 1985). The surface morphology of these active salars is complex and dynamic, and the surface crusts are shaped into a diversity of morphologies, including salt saucers, salt nodules, salt pinnacles, salt solution tubes and salt stalactites (Stoertz & Ericksen, 1974). The composition of these crusts is

variable, and includes calcium carbonate, nitrates, chloride salts, gypsum, anhydrite and other sulfates (Stoertz & Ericksen, 1974).

On the other hand, most salars along the Coastal range and in the Central Valley are hydrologically inactive, except for rare rainfalls interspersed between long periods of extreme dryness, which can last over a decade (Stoertz & Ericksen, 1974; McKay et al. 2003). These extremely dry conditions have likely persisted since the Miocene (Pueyo et al. 2001), and because these salars are not subject to seasonal or annual cycles of flooding and evaporation, we refer to them as fossil salars (Chong, 1988) to distinguish them from the active salars in the Andean front and the Altiplano. There is an almost complete absence of morphological, mineralogical and crystallographic data from this unique type of evaporitic environment.

Here we provide detailed field, microscopic and mineralogical observations of surface salt crusts from four fossil salars in the hyperarid core of the Atacama Desert. We show that the surface of these salars is dynamic on timescales of several years to decades, in response to daily cycles in atmospheric moisture, and also to rare and meager rainfall events. Our observations allow us to derive a new end-member model for the evolution of salt-encrusted playas under extreme and continuous dryness, whereby salt polygons are gradually transformed into small nodular structures due to the slow migrations of salt driven by deliquescence/efflorescence cycles.

2. Materials and Methods

2.1. Field sampling and observations

Field observations and sampling were conducted during several campaigns in May-June 2009, May 2011, and April 2013. We studied the surface morphology of four

fossil salars: Yungay, Salar de Navidad, Salar de Llamara, and Salar Grande (Figure 1).

2.2. Polarizing microscopy

Selected samples were impregnated with polyester resin for thin-section preparation prior to observation in the polarizing microscope. To prevent dissolution of the salt phases, oil was used as a lubricant during grinding. To avoid gypsum transformations, the temperature never exceeded 40°C during drying of samples for analysis and during thin-section preparation. Petrographic studies of thin sections (30-µm thick) were conducted using a Nikon Eclipse LV100Pol polarized light microscope equipped with a Nikon DS-Fi1 digital camera.

2.3. Electron microscopy

The study of thin sections under the polarizing microscope was complemented by scanning electron microscope (SEM) equipped with backscattered electron (BSE) detector. Thin sections were carbon-coated and then observed with a Quanta 3D FEG microscope (FEI Company, Hillsboro, U.S.A.) equipped with an X-ray microanalytical energy dispersive spectrometer (EDS) system (EDAX, Ametek). SEM examination in BSE detection mode and EDS microanalysis of samples were simultaneously performed. The microscopy and microanalytical operating conditions were as follows: 0º tilt angle, 35º take-off angle, 15 kV acceleration potential, 6 or 25 mm working distance and 1–5 nA specimen current.

2.4. X-ray powder diffraction (XRD)

Sample mineralogy was studied by X-ray powder diffraction (XRD), after gently powdering the samples in an agate mortar, and using a Bruker D8 ADVANCE diffractometer with graphite-monochromated CuK(a) radiation and a linear VANTEC

detector. XRD patterns were obtained from random powder mounts. For qualitative analysis of the crystalline phases present in the samples, the Power Diffraction File (PDF-2, 1999) of the International Centre for Diffraction Data (ICDD) was used. A semi-quantitative analysis of these phases was performed using the normalized reference intensity ratio (RIR) method (Chung, 1974) and the values for each phase given by the powder diffraction database (ICDD).

3. Results

3.1. Surface morphology of fossil salars

Two morphological features were pervasive on the surface of fossil salars: (1) salt polygons, and (2) salt nodules (Figure 2). Here, the term salt nodule is utilized after Stoertz & Ericksen (1974), to refer to rounded salt deposits that have formed by slow dissolution and recrystallization on surfaces of salt fragments. Salt polygons were largely subdued in some of the salars, such as Yungay, but salt nodules were conspicuous at all sites. Based on their morphology, we distinguished three general classes of polygons, classified as Type I though III (Table 1).

Type I polygons were flat and well defined with slightly elevated (i.e. 1-3 cm) rims that were sealed together with the rims of adjacent polygons (Figure 2a and 2b). These polygons contained a mixture of salt, primarily halite, and detrital particles, homogeneously distributed from the center of the polygon to the rim. Type I polygons had no associated salt nodules.

Type II polygons were characterized by a regular, concave shape, uplifted rims, and salt enrichments along polygon borders. Based on the development or maturation of salt nodules along the polygon borders, type II polygons could be subdivided as early and late stage polygons. Early stage type II polygons were relatively large (ca.

30 to 90 cm) with a lower central area and well-defined, elevated rims that formed small tepees. Occasionally, tepees of adjacent polygons were sealed together into a round polygonal rim (Figure 2c). Early stage Type II polygons showed clear structural and mineralogical differences between the polygon center (indurated, relatively porous and composed of a mixture of halite and detrital particles) and the polygon rims (significantly enriched in salt, with few detrital particles).

Late stage Type II polygons were smaller in size than early stage Type II polygons, but had elevated rims forming classic tepees (Figure 2d). Structural and mineralogical differences between the central part of the polygons and the rims were more pronounced than in the early stages. The centers of these polygons were relatively porous and composed of a mixture of halite and diverse detrital materials, whereas the tepees were often reshaped into nodular structures 5-20 cm in diameter, composed of almost pure mm-scale salt crystals with a sugary appearance (Figure 2d). Salt nodules appeared in a range of development or maturity stages. Poorly developed nodules were almost undistinguishable from tepees. Well-developed nodules were round, with an enlarged upper section and a thin long pedestal anchoring the nodule to the ground. Occasionally, adjacent nodules were conjoined, forming a small arch with two anchoring points.

Finally, Type III polygons had poorly defined borders, occasionally rounded or irregular, and were surrounded by well-developed nodules (Figure 2e and 2f). Some Type III polygons were almost vertically oriented, forming fin-like structures, and often it was difficult to differentiate the polygon center from its border (arrows in Figure 2f).

3.2. Mineralogical and crystallographic properties of salt polygons

To the best of our knowledge there have not been previous investigations of the

mineralogical and petrographic properties of the types of salt polygons described in this study. Our analyses revealed an almost conspicuous absence of crystallographic and petrographic details in the halite-rich fraction of both polygons and salt nodules. However, microscopic characterization of samples from Salar Grande and Yungay revealed a different pattern of organization and mineralogical composition between the central part of polygons, their uplifted borders and the halite nodules. Results of X-ray diffraction analyses for polygon samples are shown in Table 2.

The central parts of all types of polygons were built with a mixture of halite and detrital particles, the latter representing more than 40% of the total composition (Figure 3). Detrital particles were varied but essentially composed of quartz, feldspars and few iron oxides. The diameter of these particles was variable and up to 600μm, with a subrounded to tabular-subrounded shape. Additionally, millimeter-size pores occurred frequently within the matrix, along with anhydrite, gypsum, and celestite crystals (Figure 3). Halite in the central parts of polygons had a massive, undifferentiated aspect, and only in few regions we observed crystalline borders. In type I polygons these features were consistent throughout the polygon, but in polygon types II and III, uplifted borders displayed a higher mineralogical purity than the polygon centers and were predominantly composed of halite crystals with a minor constituent of gypsum, each mineral exhibiting both round and straight crystal sides (Figure 3g and 3h). Triple junctions with angles approaching 120º were frequently observed.

3.3. Mineralogical and crystallographic characteristics of salt nodules

The composition of salt nodules (primarily in late stage type II and type III polygons) was dominated by halite, with small anhydrite, gypsum and glauberite impurities (Table 2).

Frequently, the interior of the nodules displayed small scale banding quasi parallel to the surface of the nodule, with differences in the porosity between adjacent bands. Elongated pores sub-parallel to the nodule surface were observed in some samples, and these elongated pores were sometimes partially filled with gypsum and anhydrite (Figure 4).

Salt nodules in type III polygons displayed the highest degree of maturity, based on mineralogical and crystallographic features. The upper section of these nodules was often rich in detrital particles (e.g., quartz, feldspar). However, these grains were markedly absent in other parts of the nodule (Figure 5), which were instead composed of almost pure halite with embedded gypsum particles. In addition, these nodules typically had a clearly defined inner structure: (1) a porous interior core several centimeters in diameter that contained mm size cavities; (2) a surrounding layer of almost pure halite crystals with a sugary appearance (average pore radius 153.10 nm reported by Wierzchos et al. (2012)); and (3) a dense outer shell a few millimeters thick, composed almost exclusively of halite (Figure 6). At the micro scale, this outer layer appeared massive, with very small or no pore spaces (average pore size of 42.6nm reported by (Wierzchos et al. 2012)), and typically contained hollow-faced halite crystals (Figure 6f). The same zonation was already noted by Wierzchos et al. (2012) based on mercury porosimetry analyses and light and SEM observations. This zonation was less evident in nodules from Type II polygons.

4. Discussion

The majority of morphological, mineralogical and petrographic studies in evaporitic environments have focused on active systems such as deep perennial basins, shallow perennial lakes and ephemeral saltpans (Lowenstein and Hardie, 1985).

Here, crystallographic and petrographic criteria have shed light on the primary depositional fabrics and possible diagenetic and post-depositional transformations of salt deposits (Shearman, 1978; Arthurton, 1973; Lowenstein and Hardie, 1985; Casas and Lowenstein, 1989; Smoot and Lowenstein, 1991). For example, the presence of xenotopic halite with triple junction grain boundaries approaching 120º angles was considered by Hardie et al. (1985) as an indicator of re-crystallization processes. However, Bein et al. (1990) already recognized the challenges when attempting to differentiate depositional from diagenetic fabrics in halite deposits. In the case of fossil salars, there is a conspicuous absence of published data available on the primary depositional fabrics and possible diagenetic features and post-depositional transformations, which complicated our field and laboratory observations. In the following section we argue that the microscopic features observed on the surface of fossil salars are primarily related to post-depositional transformations (i.e. dissolution and re-precipitation). We posit that these post-depositional transformations, and the polygonal and nodular morphologies observed on the surface of fossil salars, can only occur under extreme and prolonged dryness.

4.1. Genesis and evolution of halite polygons

Salt polygons are frequently found in continental evaporitic environments that contain brine concentrations near the surface (Neal, 1975). These polygons are characterized by their uplifted borders (pressure ridges), which form through a process of lateral salt displacement (Christiansen, 1963; Shearman, 1978; Lines, 1979; Beydoun, 1980; Tucker, 1981; Fryberger et al., 1983; Lowenstein and Hardie, 1985; De Deckker, 1988; Keheila et al., 1989; Bobst et al., 2001) due to crystallization pressures (Handford, 1991), or to thermal contraction and expansion (Dellwig, 1968; Tucker, 1981; Handford, 1991). The durability of salt polygons in

most evaporitic environments is limited by seasonal rainfall or flooding events, which destroy the surface morphology and initiate a new cycle of polygon formation and evolution.

A unique feature of fossil salars in the Atacama Desert is that long periods (decades or longer) of extreme dryness separate short and meager rainfalls. As a result, the surface of the salars remains in the desiccation stage for much longer than in other evaporitic environments. Yet, our field observations show that even in this extreme dryness the surface crust of the salars is dynamic and continues to change, albeit at slower rates.

The macro-morphology of polygons at the study sites, as well as the mineralogical and crystallographic characteristics of each type of polygon and salt nodule, can be interpreted as a continuum in the evolution of salt polygons under extreme and prolonged dryness (Figure 7). The process is initiated with the migration of salt from the center of polygons towards the borders though lateral salt displacement. As a result, type I polygons, which are homogeneous in composition and fabric both horizontally and in cross-section, slowly evolve into type II polygons whose borders are enriched in halite and depleted in detrital materials (Figure 2c and Figure 3). The presence of abundant mm-size pores in the central parts of type II polygons supports the idea of mass loss due to salt displacement, leaving behind void spaces in a siliciclastic matrix. Type III polygons represent an extreme case of lateral salt displacement resulting in the uplift of the entire polygon body and separation from the soil below (Figure 2f).

The evolution of polygons from type I to type III is likely driven by episodic rainfall and fog events, as well as salt deliquescence process, which in certain cases is preceded by water vapor capillary condensation (Wierzchos et al. 2012). These wet

episodes are sufficient to drive the migration of salt, but not sufficiently intense to completely dissolve the salt crust. Comparisons between salars support the notion that the evolution of each polygon type is controlled by moisture availability. Type I polygons are present in all salars, but in low numbers. Type II polygons (both early and late stages) dominate in Salar Grande and Salar de Llamara, which are the "wettest" localities, which have a mean annual relative humidity (RH) of 50-60% and relatively frequent fog events due to their proximity to the Coastal Cordillera (Robinson et al., 2013). In Salar Llamara moisture is also frequent'wet' due to high values of (RH) and localized regions with a shallow water table. Type III polygons are most prevalent in Yungay, the driest locality, which has a mean annual RH of 35% (Robinson et al. 2013), and rare fog events (McKay *et al.* 2003; Caceres *et al.* 2007). Salar de Navidad occupies an intermediate position. We speculate that the relatively humid conditions in Salar Grande and Salar de Llamara favor the development of type II polygons, but interfere with the development of type III polygons, which requires even drier conditions, such as occur in the Yungay region. Indeed, since 1994 there have been three registered instances of atmospheric precipitation in the Yungay area. McKay *et al.* (2003) reported a sporadic rain event of 2.3 mm that resulted in moist soil for a total of 65-85 hours. Our own monitoring of microclimate parameters (Wierzchos et al. (2012) registered RH of 100% during 5 hours in 2006, perhaps linked to a rain event or heavy fog. In July 2011 a rainfall gauge measured 5 mm of precipitation. We posit that these exceedingly dry conditions punctuated by meager rainfall events or fog, deliquescence and capillary condensation are necessary to drive the evolution of polygons all the way to type III.

A localized leak in a water pipe running across Yungay area from pump station to the Aguas Blancas mining company in 2006 allowed us to constrain the time required for

polygons to evolve from Type I to Type II. The water leak resulted in a small surface pond that dissolved a small area of the evaporitic deposits, thereby erasing parts of the surface morphology (Figure 8). One year after the formation of the new salt crust the surface was largely composed of Type I polygons, but in 2011, four years later, the surface of the crust had already evolved into a well-defined pattern of salt polygons with uplifted borders occasionally forming tepees and salt nodules up to 5 cm in diameter, and covered with a brown layer of wind-blown detrital particles (i.e. Type II polygons had formed).

4.2. Development of halite nodules.

The borders of the polygons are reshaped into round nodules during the development of type II and type III polygons (Figure 7-V and VI). The nodules around type II polygons appear to have a different internal structure and a different degree of development than the nodules around type III polygons (see section 3.3). Field observations show that the surfaces of the nodules are dynamic and that salt is redistributed within and on the nodules. The clearest evidence of salt redistribution on the surface of nodules is fresh efflorescence (Figure 5f) pointing to recent salt dissolution and re-precipitation, and the presence of salt stalactites on the underside of well-developed nodules, suggesting brine movement and seepage (Figure 9). Widespread remains of past salt mining activity can be found in all fossil salars in the form of metal artifacts covered in rust. These metal pieces are often covered by or embedded within large salt nodules, as shown in Figure 8f. While the last timing of mining activity in the salars is difficult to constrain, most of them have been inactive since the 1950s or earlier, suggesting that the nodules are reshaped and can grow around, or over relatively modern artifacts. This was confirmed with a field experiment that consisted of covering a salt nodule in Salar Grande with sterile

gauze (Figure 9). Over a course of 2 years the swab was almost completely covered in a fresh white halite efflorescence, pointing to an active process of salt dissolution and re-precipitation over relatively short periods of time (months to years).

Taken together, the above field observations suggest that the formation and evolution of salt nodules along polygon borders is slow compared to the evolution of the polygons themselves. Small nodules first form from polygon tepees on timescales of several years, but the nodules remain dynamic and their shape evolves via gentle salt dissolution, transport and re-precipitation over timescales of decades, as indicated by the presence of fresh efflorescence on the halite nodules and the gauze experiment.

Halite nodules in type III polygons typically have a defined inner structure with three distinct regions that can be clearly differentiated based on mineralogy and crystal fabric (Figure 6), as well as by their differences in pore space distribution (Wierzchos *et al.,* 2012). We postulate that this internal structure reflects the late stage evolution of the salt nodules, and can be explained by a wetting process driven by deliquescence. When the RH in the environment rises above the deliquescent point of halite (RH>75%) liquid water condenses in the interior of the halite nodule (Figure 10). This has been shown to occur in Yungay area during the nighttime, when atmospheric temperatures drop, sometimes close to freezing (Davila et al., 2008; Wierzchos *et al.,* 2012). Deliquescence leads to a partial dissolution of the interior of the salt nodule, and the formation of large pores and cavities (Figure 6). Another demonstrated source of liquid water is spontaneous capillary condensation at relative humidity (RH) much lower than the deliquescence RH (DRH) of NaCl (Wierzchos et al. 2012). This condensation could occur inside nano-pores smaller than 100 nm. The presence of these nano-pores would theoretically allow for

capillary water condensation at RH<DRH (i.e. 50–55% instead of 75 %), and for water retention for prolonged periods of time. As temperatures on the surface of the nodules increase after sunrise (up to 40-50ºC) the internal moisture accumulated during the night will migrate towards the outer layers of the nodule driven by capillarity and evaporation processes (Figure 10). As water evaporates rapidly near the surface of the nodules, temperature of nodule is decreasing leading to the water condensation and NaCl precipitates forming a dense outer layer, 5-10 mm thick, with small pore spaces (Figure 6). Wind action might contribute to the evolution of salt nodules in two different ways: (1) by accelerating evaporation on the surface of the nodule and enhancing the movement of water from the interior of the nodule towards the surface; and (2) by abrading and eroding the salt nodules with entrained sand particles. Fin-like structures in type III polygons (Figure 2f) are likely examples of nodule (and polygon) erosion by wind action.

The successive growth layers of the nodule are made visible by the presence of internal laminae, which are parallel to the external surface of each nodule (Figure 10). The presence of hollow-faced crystals in the outer layer of the nodules (Figure 6), similar to those found by Buck *et al.* (2006) in soils from Las Vegas Wash, point to a process of rapid precipitation from a supersaturated solution due to intense evaporation. An analogous process has been proposed to explain similar crystalline halite morphologies on the surface of an ornamental porous limestone after evaporation of a brine solution (Rodriguez-Navarro et al. 2002). Other authors (Joeckel et al. 1999) found similar morphologies in surface salt crusts, which were interpreted as partially dissolved halite crystals. However, the mechanism responsible for the preferential dissolution of certain crystal planes was not proposed. We interpret the morphology of the hollow-faced halite crystals as an

indication of salt precipitation from saturated brine, resulting in skeletal crystals with cubic and prismatic shapes. The round aspect of the halite crystals would then be a result of subsequent partial dissolution due to the presence of water between crystals. Finally, Hovorka *et al.* (2007) proposed that the surface of saltpans is subject to hygroscopic alteration that reduces crystal size and increases cementation. Cycles of dissolution followed by rapid evaporation and salt precipitation would explain the small size of the halite crystals in this outer layer (Lokier, 2012).

Different sources of water, such as rainfall and fog, can alter the formation and evolution of salt nodules, and be responsible for some of other dissolution features observed on the surface of the nodules (Figure 6b), as well as the pattern of large pores sub-parallel to the surface (Figure 4). However, rainfall and fog events are so infrequent and sparse in the hyperarid core of the Atacama that they are unlikely to play a significant role in the long-term evolution of the nodules. The presence of the nodules themselves speaks against substantial surface ponding or flooding, which would dissolve and destroy the nodules, and argues instead for a slow formation mechanism that is able to mobilize salt but at the same time preserves the structures. Deliquescence and capillary condensation of water vapor provide this "goldilocks" amount of liquid water, and in addition provide sufficient liquid water to sustain the endolithic communities of phototrophic and heterotrophic microorganisms inside the nodules (Wierzchos et al., 2006; de los Ríos et al., 2010; Davila et al., 2008; Wierzchos et al., 2012; Davila et al., 2013; Robinson et al. 2013). While halite endoliths must still be adapted to stress conditions inside the halite nodules (i.e. low water activity due to high salinity), hygroscopic salts such as halite become oasis for life in extremely dry environments, when all other survival strategies fail. To the best

of our knowledge the halite nodules formed by the described processes in the extremely hyper-arid zone of the Atacama Desert are the unique habitats where life can be possible.

5. Conclusions

Surface morphologies in hydrologically inactive fossil salars detached from groundwater brines are interpreted here as an end stage in the evolution of evaporitic deposits under extreme and prolonged dryness. The surface of these fossil salars is characterized by polygonal shapes with nodular structures along their sides. The morphology and bulk mineralogy of salt polygons differs between and within salars, and the shape and internal structure of salt nodules varies between different polygon types. We propose that rare rainfall events are responsible for the differential displacement of salt from the center to the border of desiccation polygons, and the partial dissolution of salt nodules along polygon borders. On the other hand, frequent, but less intense, deliquescence and capillary condensation results in brine water condensing in the interior of nodules, leading to partial dissolution of the salt fabric and the formation of large pore spaces. Deliquescence brine migrates outward from the center of the nodules, following thermal and humidity gradients. Rapid evaporation of the brine fluids near the surface results in the observed layered structure, small porosity and characteristic crystal morphologies. Hence, despite extreme dryness, the surfaces of fossil salars are dynamic on timescales of several years to decades, in response to daily cycles in atmospheric moisture, and also to rare and meager rainfall events. Wind likely plays an important role in the formation and evolution of the nodules, both as an erosive agent and by increasing the evaporation rates of deliquescence brines near the surface of the nodules. However, its relative importance on the evolution of the

nodules is difficult to evaluate. We propose that fossil salars in the Atacama Desert represent an end stage in the evolution of evaporitic deposits under extreme and prolonged dryness.

Acknowledgments

Technical support was provided by SAIUEX for the XRD analyses and Scanning electron microscopy study. This work was funded by grant CGL2010-16004 and CGL2013-42509 from the Spanish Ministry of Science and Innovation. A.F.D., O.A. and J.W. were supported by Grant NNX12AD61G of the NASA Astrobiology program. P.B. was supported by the Thomas J. Watson Foundation.

References

Arthurton RS. 1973. Experimentally produced halite compared with Triassic layered halite-rock from Cheshire, England. *Sedimentology* **20**: 145-160.

Bein A, Hovorka SD, Fisher RS, Roedder E. 1990. Fluid inclusions in bedded Permian halite, Palo Duro Basin, Texas: evidence for modification of seawater in evaporite brine-pools and subsequent early diagenesis. *Journal of. Sedimentary Petrology* **61 (1)**: 1-14.

Beydoun ZR. 1980. Some holocene geomorphological and sedimentological observations from Oman and their palaeogeological implications. *Journal of Petroleum Geology* **2(4)**: 427-437.

Bobst AL, Lowenstein TK, Jordan TE, Godfrey LV, Ku T-L, Luo S. 2001. A 106 ka paleoclimate record from drill core of the Salar de Atacama, northern Chile. *Palaeogeography, Palaeoclimatology, Palaeoecology* **173**: 21-42.

Buck BJ, Wolff K, Merkler DJ, McMillan NJ. 2006. Salt mineralogy of Las Vegas Wash, Nevada: morphology and subsurface evaporation. *Soil Science Society of America Journal* **70**: 1639-1651.

Cáceres L, Gómez-Silva B, Garró X, Rodríguez V, Monardes V, McKay CP. 2007. Relative humidity patterns and fog water precipitation in the Atacama Desert and biological implications. *Journal of Geophysical Research* **112**, G4S14. DOI: 10.1029/2006JG000344.

Casas E, Lowenstein TK. 1989. Diagenesis of saline pan halite: comparison of petrographic features of Modem, Quaternary and Permian halites. *Journal of Sedimentary Petrology* **59** (5): 724-739.

Chong G. 1988. The Cenozoic saline deposits of the Chilean Andes between 18° and 27° South. In *The southern Central Andes*. H. Bahlburg H, Breitkreuz C, Giese P (eds.). Springer-Verlag. 135-151.

Chung FH. 1974. Quantitative interpretation of X-ray-diffraction patterns of mixtures. II. Adiabatic principle of X-ray-diffraction analysis of mixtures. *Journal of Applied Crystallography* **7**: 526-531.

Christiansen FW. 1963. Polygonal fracture and fold systems in the salt crust, Great Salt Lake desert, Utah. *Science* **139**: 607-609.

Clarke J. 2006. Antiquity of aridity in the Chilean Atacama Desert. *Geomorphology* **73** (1-2): 101-114.

Davila AF, Gómez-Silva B, de los Ríos A, Ascaso C, Olivares H, McKay CP, Wierzchos J. 2008. Facilitation of endolithic microbial survival in the hyperarid core of the Atacama Desert by mineral deliquescence *Journal of Geophysical Research* **113**. G01028. DOI:10.1029/2007JG000561.

Davila AF, Hawes I, Ascaso C, Wierzchos J. 2013. Salt deliquescence drives photosynthesis in the hyperarid Atacama Desert. *Environmental Microbiology Reports* **5**: 583–587. DOI: 10.1111/1758-2229.12050

De Deckker P. 1988. Biological and sedimentary facies of Australian salt lakes. *Palaeogeography, Palaeoclimatology, Palaeoecology* **62**: 237-270.

de los Ríos, A., Valea, S., Ascaso, C., Davila, A., Kastovsky, J., McKay, C.P., Gómez-Silva, B., and Wierzchos, J. (2010). Comparative analysis of the microbial communities inhabiting halite evaporites of the Atacama Desert. *International Microbiology* **13**: 79-89. DOI: 10.2436/20.1501.01.113.

Dellwig LF. 1968. Significant features of deposition in the Hutchinson Salt, Kansas, and their interpretation. *Geological Society of America Special Paper* **88**: 421-427.

Dunai TJ, González-López GA, Juez-Larré J. 2005. Oligocene-Miocene age of aridity in the Atacama Desert revealed by exposure dating of erosion-sensitive landforms. *Geology* **33**: 321-324.

Ericksen GE. 1983. The Chilean nitrate deposits. *American. Scientist* **71** (4): 366–374.

Ericksen GE, Salas R. 1990. Geology and resources of salars in the Central Andes. In *Geology of the Andes and Its Relation to Hydrocarbon and Mineral Resources*. Ericksen GE, Cañas MT, Reinemund JA (eds.). Circumpacific Council for Energy and Mineral Resources., Earth Science Series, V. 11; 165-172.

Fryberger SG, Al-Sari AM, Clisham TJ. 1983. Eolian dune, interdune, sand sheet, and siliciclastic sabkha sediments of an offshore area, Dhahran Area, Saudi Arabia. *American Association of Petroleum Geologist Bulletin* **67**: 280-312.

Handford CR. 1991. Marginal Marine Halite: Sabkhas and Salinas. In *Evaporites, Petroleum and Mineral Resources*. Developments in Sedimentology. Elsevier; 1-66.

Hardie LA, Lowenstein TK, Spencer RJ. 1985. The problem of distinguishing between primary and secondary features in evaporites. In *Sixth Inter. Symposium on Salt*. Schreiber BC, Harner HL (eds.). The Salt Institute, Alexandria, Virginia; 11–39.

Houston J, Hartley AJ. 2003. The central Andean west-slope rainshadow and its potential contribution to the origin of hyper-aridity in the Atacama Desert. *International Journal of Climatology* **23**: 1453–1464.

Hovorka SD, Holt RM, Powers DW. 2007. Depth indicators in Permian Basin evaporites. In *Evaporites Through Space and Time* .Schreiber BC, Lugli S, Babel M (eds.). Geological Society, London, Special Publications, 285; 335-364.

Joeckel RM, Clement BA. 1999. Surface features of the Salt Basin of Lancaster County, Nebraska. *Catena* **34**: 243-275.

Keheila E, Khalifa H, El-Haddad A. 1989. Holocene carbonate facies model, Ras Shukhier hypersaline pool and its surrounding sabkha, west Gulf of Suez, Egypt. *Sedimentary Geology* **63**: 155-169.

Lines GC. 1979. *Hydrology and surface morphology of the Bonneville Salt Flats and Pilot Valley, Utah*. U.S. Geological Survey, Washington, DC, USA. Water-Supply Paper 2057.

Lokier SW. 2012. Development and evolution of subaerial halite crust morphologies in a coastal sabkha setting. *Journal of Arid Environments* **79**: 32-47.

Lowenstein TK, Hardie LA. 1985. Criteria for the recognition of salt-pan evaporites.

Sedimentology **32**: 627-644.

McKay CP, Friedmann EI, Gómez-Silva B, Cáceres-Villanueva L, Andersen DT, Landheim R. 2003. Temperature and moisture conditions in the extreme arid regions of the Atacama Desert: four years of observations including the El Niño of 1997–1998. *Astrobiology*, **3**:393–406.

Neal JT. 1975. *Playas and dried lakes: occurrence and development*. Stroudsburg, Pa: Dowden, Hutchinson & Ross.

Pueyo JJ, Chong G, Jensen A. 2001. Neogene evaporites in desert volcanic environments: Atacama Desert, northern Chile. *Sedimentology* **48**: 1411-1431.

Robinson CK, Wierzchos J, Black C, Crits-Christoph A, Ma B, Ravel J, Ascaso C,Artieda O, Valea S, Roldan M, Gomez-Silva B, Diruggiero J. 2013. Microbial diversity and the presence of algae in halite endolithic communities are correlated to atmospheric moisture in the hyper-arid zone of the Atacama Desert. *Environmental Microbiology*. DOI:10.1111/1462-2920.12364

Rodriguez-Navarro C, Linares-Fernandez L, Doehne E, Sebastian E. 2002. Effects of ferrocyanide ions on NaCl crystallization in porous stone. *Journal of Crystal Growth* **243**: 503-516.

Shearman DJ. 1978. Evaporites of coastal sabkhas. In *Marine Evaporites*. Dean WE, Schreiber BC (eds.). SEPM Short Course No. 4. Society for Sedimentary Geology; 6-42.

Smoot JP, Lowenstein TK. 1991. Depositional environments of non-marine evaporites. In *Evaporites, Petroleum and Mineral Resources*. Melvin JL (ed.). Developments in Sedimentology 50. Elsevier Science Publishers B.V., Amsterdam, Holland; 189–347.

Stoertz GE, Ericksen GE. 1974. *Geology of salars in northern Chile*. U.S. Geological Survey, Professional Paper, No. 811.

Tucker RM. 1981. Giant polygons in the Triassic salt of Cheshire, England: a thermal contraction model for their origin. *Journal of Sedimentary Petrology* **51**: 779-786.

Wierzchos J, Ascaso C, McKay CP. 2006. Endolithic cyanobacteria in halite rocks from the hyperarid core of the Atacama Desert. *Astrobiology* **6** (3): 415-422.

Wierzchos J, Davila AF, Sánchez-Almazo IM, Hajnos M, Swieboda R, Ascaso C. 2012. Novel water source for endolithic life in the hyperarid core of the Atacama Desert. *Biogeosciences* **9**: 2275-2286.

Tables:

Table 1. Morphological classification of salt polygons in fossil salars.

Polygon Type	Shape/Aspect	Polygon borders	Salt nodules	Interpretation
I	Regular Flat	Flat Open troughs or sealed Undifferentiated	Not present	Initial stage of dry salt encrusted playa. Can become a remnant feature due to salt starvation
II- Early stage	Regular Concave	Slightly uplifted Incipient tepees Open troughs or sealed Enriched in salt	Incipient	Initial stage of polygon evolution from lateral salt displacement.
II- Late stage	Regular Concave	Well-developed tepees Open troughs Enriched in salt	Mature	Advanced stage of polygon evolution from lateral salt displacement.
III	Irregular Uplifted Fin-like	Round Heavily uplifted Highly deformed Enriched in salt	Mature. Distinct internal zonation	Final stage of polygon evolution from lateral salt displacement.

Table 2. Semi-quantitative mineralogical composition from any samples of polygons and nodules samples determined by XRD.

Location	Sample	Mineral composition					
		Halite	Glauberite	Gypsum	Anhydrite	Quartz	Calcite
Polygons							
Yungay	ATAC-36	+++	-	++	++	+	-
Salar Grande	ATAC-32	++++	-	+	-	-	-
	ATAC-33	++++	-	-	-	+	-
Salt nodules							
Yungay	ATAC-4	+++	++	-	+	+	-
	ATAC-4B	+++	-	+	++	+	+
Navidad	ATAC-05	++++	-	+	-	-	-
	ATAC-310b	++++	-	-	-	-	-
Llamara	ATAC-21	++++	-	+	-	-	-
Salar Grande	ATAC-29	++++	-	+	-	-	-

++++ (>95%); +++(50%-94%); ++ (10%-49%); + (<9%); - (not detected)